

RESEARCH ARTICLE

Comparative experimental evolution reveals species-specific idiosyncrasies in marine phytoplankton adaptation to warming

Samuel Barton^{1,2}  | Daniel Padfield¹  | Abigail Masterson¹ | Angus Buckling¹  |
Nicholas Smirnoff³  | Gabriel Yvon-Durocher¹ 

¹Environment and Sustainability Institute, University of Exeter, Penryn Campus, Penryn, UK

²Department of Earth Sciences, University of Oxford, Oxford, UK

³Biosciences, College of Life and Environmental Sciences, University of Exeter, Exeter, UK

Correspondence

Samuel Barton and Gabriel Yvon-Durocher, Environment and Sustainability Institute, University of Exeter, Penryn Campus, Penryn, Cornwall TR10 9FE, UK. Email: samuel.barton@earth.ox.ac.uk and g.yvon-durocher@exeter.ac.uk

Funding information

Leverhulme Trust, Grant/Award Number: RPG-2013-335

Abstract

A number of experimental studies have demonstrated that phytoplankton can display rapid thermal adaptation in response to warmed environments. While these studies provide insight into the evolutionary responses of single species, they tend to employ different experimental techniques. Consequently, our ability to compare the potential for thermal adaptation across different, ecologically relevant, species remains limited. Here, we address this limitation by conducting simultaneous long-term warming experiments with the same experimental design on clonal isolates of three phylogenetically diverse species of marine phytoplankton; the cyanobacterium *Synechococcus* sp., the prasinophyte *Ostreococcus tauri* and the diatom *Phaeodoactylum tricornutum*. Over the same experimental time period, we observed differing levels of thermal adaptation in response to stressful supra-optimal temperatures. *Synechococcus* sp. displayed the greatest improvement in fitness (i.e., growth rate) and thermal tolerance (i.e., temperature limits of growth). *Ostreococcus tauri* was able to improve fitness and thermal tolerance, but to a lesser extent. Finally, *Phaeodoactylum tricornutum* showed no signs of adaptation. These findings could help us understand how the structure of phytoplankton communities may change in response to warming, and possible biogeochemical implications, as some species show relatively more rapid adaptive shifts in their thermal tolerance.

KEYWORDS

climate change, experimental evolution, phytoplankton, thermal adaptation, thermal tolerance, warming

1 | INTRODUCTION

It is expected that warming could directly drive reductions in marine primary production due to loss of diversity and possible extinctions of phytoplankton taxa, particularly at lower latitudes, where temperatures may exceed thermal tolerance limits (Bestion et al., 2020; Thomas et al., 2012, 2016). This is especially true when

environmental temperatures are frequently in the supra-optimal range of species' thermal tolerance (i.e., temperatures beyond thermal optima of growth), meaning they are more vulnerable to periods of extreme warming or heatwaves (Anderson et al., 2021; Baker & Geider, 2021; Thomas et al., 2012). The dominant functional traits that emerge from the response of phytoplankton communities to warming are likely to have knock-on implications for primary

This is an open access article under the terms of the [Creative Commons Attribution](https://creativecommons.org/licenses/by/4.0/) License, which permits use, distribution and reproduction in any medium, provided the original work is properly cited.

© 2023 The Authors. *Global Change Biology* published by John Wiley & Sons Ltd.

production and biogeochemical cycles (Anderson et al., 2021; Dutkiewicz et al., 2013). For example, shifts to a greater prevalence of smaller cells, particularly cyanobacteria and eukaryotic picophytoplankton (cells <2 µm diameter, Raven, 1998), could have a diminishing effect on the biological carbon pump due to lower sinking velocities relative to heavier cells, such as diatoms, resulting in a reduced flux of carbon to the oceans interior (Falkowski et al., 1998; Litchman & Klausmeier, 2008; Morán et al., 2010).

In recent years, there has been a drive to understand whether marine phytoplankton can mitigate some of the projected local extinctions and compositional turnover through evolutionary adaptation to warming (Aranguren-Gassis et al., 2019; Baker et al., 2018; Jin & Agustí, 2018; Listmann et al., 2016; O'Donnell et al., 2018; Padfield et al., 2016; Pierangelini et al., 2020; Schaum et al., 2018; Schlüter et al., 2014). Generally, long-term selection experiments have demonstrated that phytoplankton can rapidly adapt, over 100 generations or more, to both warmed and fluctuating temperature environments, and this is often characterized by an improvement in fitness (or growth rate), in response to elevated temperatures. Thus far, work has been limited to a couple of model species of freshwater green algae, *Chlorella vulgaris* and *Chlamydomonas reinhardtii* (Padfield et al., 2016; Schaum et al., 2017), and a handful of marine taxa covering just three key functional types; the diatoms *Thalassiosira pseudonana* (O'Donnell et al., 2018; Schaum et al., 2018), *Chaetoceros simplex* (Aranguren-Gassis et al., 2019) and *Skeletonema dohrnii* (Cheng et al., 2022), the coccolithophore *Emiliania huxleyi* (Listmann et al., 2016; Schlüter et al., 2014), and the dinoflagellate *Amphidinium massartii* (Baker et al., 2018). While all of these studies have been insightful for understanding thermal adaptation at the individual species level, all of them have focussed on only a single species. Critically, although they generally find that phytoplankton can shift their thermal tolerance in response to warming, comparing results across studies and taxonomic groups is difficult owing to the difference in timescale of the experiments (years vs. months), differing levels of thermal stress (magnitude of the temperature relative to the species' optimal temperature of growth) and other nuances of the experimental designs (e.g., starting experiments from clonal or non-clonal populations). To gain greater clarity in our understanding of differences in adaptive potential across functional groups, it is therefore necessary for standardized experimental studies (see Jin & Agustí, 2018 for an example of such an experimental approach in diatoms from the Red Sea), which would allow us to make more meaningful assertions about how phytoplankton community structure will change following potential adaptive responses to warming.

To fill this knowledge gap, this study investigates the magnitude of thermal adaptation for three ecologically relevant marine phytoplankton species, representing different functional groups, using the same standardized experimental protocol (see Figure 1). Simultaneous long-term warming experiments were conducted on clonal replicates of *Synechococcus* sp.—a globally abundant cyanobacterium (Flombaum et al., 2013; Pittera et al., 2014), *Ostreococcus tauri*—a prasinophyte and the smallest known eukaryote (Courties et al., 1994; Derelle et al., 2006), and *Phaeodactylum tricornutum*—a prevalent diatom in coastal marine ecosystems (Heydarizadeh et al., 2017; Zhao et al., 2014). Previous long-term warming studies on phytoplankton tend to use the number

of generations to infer adaptive changes, with evolutionary responses often observed within ~100 generations (Padfield et al., 2016; Schaum et al., 2018; Schlüter et al., 2014). Here, we used a set period of time to investigate adaptation in response to similar supra-optimal thermal stress across the species. This approach allowed for intrinsic differences in average generation time across the three species to impact the amount of thermal adaptation observed over the set time period. Following adaptation to supra-optimal temperatures, we measured the thermal tolerance curves of growth, for both the ambient and warmed treatment lineages of each species. We also quantified key morphological and biochemical traits (including average cell size, and per capita carbon, nitrogen and chlorophyll *a*) to further understand the possible implications of thermal adaptation on the biogeochemical functioning of the organisms.

2 | MATERIALS AND METHODS

2.1 | Culture conditions and experimental design

The strains of *Synechococcus* sp. (CCMP 2370, WH8102) and *Ostreococcus tauri* (RCC 4221) were originally obtained from RCC (Roscoff Culture Collection), and the strain of *Phaeodactylum tricornutum* (CCAP 1052/1B, CCMP 2558) from CCAP (The Culture Collection of Algae and Protozoa). Stock cultures of each of the three species in this study had been maintained in the lab under similar conditions to those of their respective culture collection for a minimum of 1 year before the experiment commenced. Cultures were kept under nutrient replete conditions at an ambient temperature of 20°C, on a 12:12 h light-dark cycle at approximately 45–50 µmol m⁻² s⁻¹ and at a constant agitation of 65 r.p.m in an Infors HT incubator. Each of the strains was grown on their long-term culture collection mediums; PCR-S11 for *Synechococcus* sp., Keller's K for *Ostreococcus tauri* and Guillard's F/2 + Si for *Phaeodactylum tricornutum*. Before starting the experiment, we identified 'stressful' high temperatures to be used for our warmed treatments by obtaining thermal tolerance curves for each of the species. This was achieved by measuring growth rate for three technical replicates across a range of nine assay temperatures, from 18°C to 33°C (see Section 2.5 for details on measuring growth rates and modelling the thermal tolerance curves, Figure 1b, and results). From the modelled thermal tolerance curves of the pre-clonal stock populations, we identified a supra-optimal temperature for each of the species where rates were approximately 50% lower than maximal growth rates (r_{max}^{40}); for *Synechococcus* sp., this was 30°C; for *Ostreococcus tauri*, 33°C; and for *Phaeodactylum tricornutum*, 27°C, (see step (1) in Figure 1a,b). By taking this approach, we had a quantitative justification for the selection of the high-temperature treatments, allowing us to make more informative comparisons of the extent of observed thermal adaptation across the species over a set time period. Furthermore, while these temperatures might be considered fairly high, it is worth noting that many phytoplankton taxa already persist in environments where the average annual temperature is supra-optimal, and a great deal more have incredibly narrow thermal safety margins (Anderson et al., 2021; Thomas et al., 2012), thereby making comparisons of

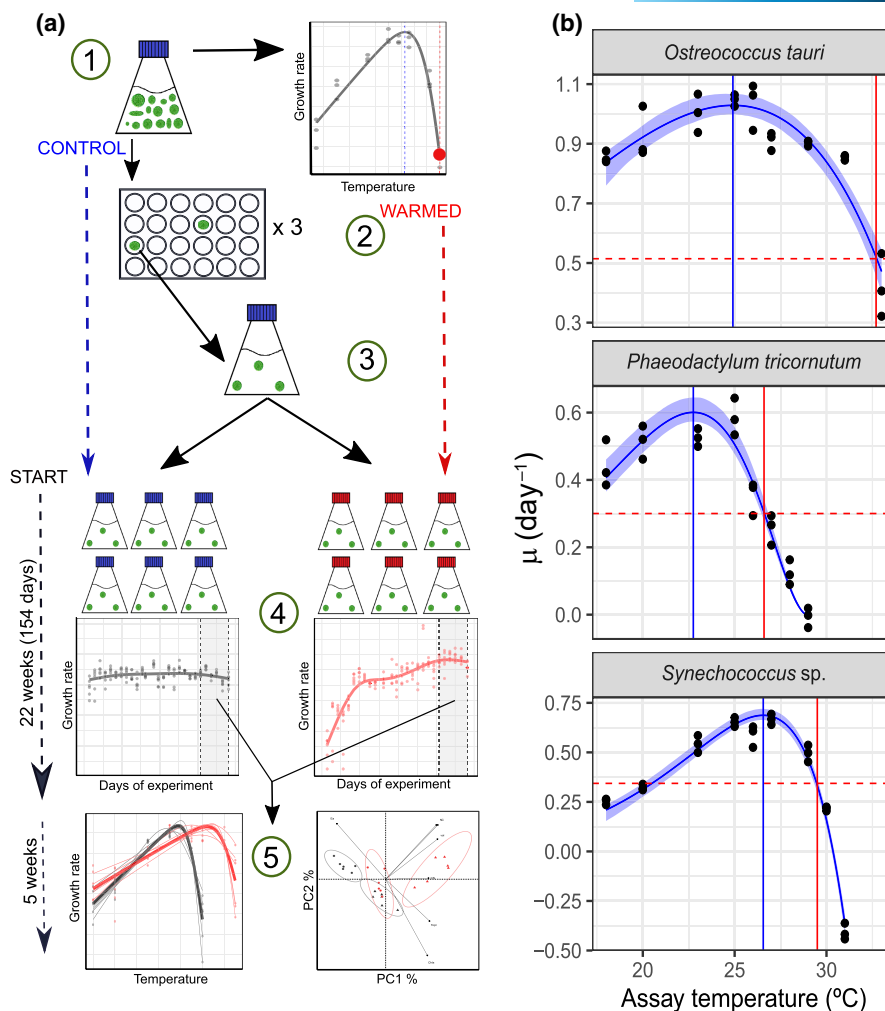


FIGURE 1 (a) Schematic diagram of the experimental design for each species. (1) We determined suitable supra-optimal warming temperatures where growth rates were ~50% of the maximal rate for pre-clonal stock populations of each species. (2) We obtained single clonal starting populations for each species following a serial dilution-to-extinction method. (3) The clonal population was distributed into six biological replicates at both the control temperature (20°C) and the supra-optimal temperature selected for each species. (4) We maintained the biological replicates through regular weekly subculturing and monitored the long term trajectories of population growth rate. (5) After a 22-week period, we measured the thermal tolerance curves of all biological replicates from each treatment, as well as measuring a number of other functional traits (e.g., per cell carbon and nitrogen quotas). For a more detailed description of each step in the schematic (1–5), see Section 2.1. (b) Thermal tolerance curves of pre-clonal stock populations. Data points represent specific growth rates (μ) for a minimum of three technical replicates per assay temperature. Fitted blue lines represent the thermal tolerance curves, and shading represents the 95% confidence interval of the selected model fits. The solid blue vertical line highlights the thermal optima (T_{opt}^{μ}) for each of the species. Supra-optimal temperature where rates were approximately 50% of the maximal rate for each species is highlighted by the intersect between the solid and dashed red lines; 33°C for *Ostreococcus tauri*, 27°C for *Phaeodactylum tricornutum* and 30°C for *Synechococcus* sp. (see Table S1).

adaptive potential to supra-optimal temperatures a highly necessary research frontier in the face of climate change and ocean warming.

We obtained clonal starting populations for each of the species by serial dilution-to-extinction, in three 24-well plates for each species with an approximation of one individual inoculated per well (see step (2) in Figure 1a). Once clonal growth was evident, we chose a single clonal population at random for each of the species to be the ancestral population for our experiment. The clonal ancestor was distributed into six replicates at both the ambient control temperature, 20°C, and the identified high-temperature treatment for each species (see step (3) in Figure 1a). With exception to the change in temperature for the warmed treatments, culturing conditions were

kept as they were for the original stock cultures (as described above). The biological replicates at each temperature were maintained by transferring cells to fresh sterile medium on a weekly basis during the exponential growth phase, back to the same original starting density in 100 mL for each species. If cultures had not grown beyond the initial starting density, or had declined, then a weekly transfer was not made. Species-specific starting densities were calculated to ensure that all cultures stayed in exponential growth over the period of 1 week. This allowed for calculation of specific growth rates between transfers, as well as changes in population density to be observed for both the control and warm-adapted cultures (see step (4) in Figure 1a). After an experimental period of 22 weeks, all additional

physiological data were collected over an additional 5-week period for each of the biological replicates, including measurements of thermal tolerance curves, and per capita mass of organic carbon, nitrogen, and chlorophyll *a* (see step (5) in Figure 1a).

2.2 | Flow cytometry

We used an Accuri C6 flow cytometer (BD Scientific) to measure population density of our experimental replicates, where living populations of cells were identified by FL3 channel fluorescence (i.e., chlorophyll *a* emission at 670nm). Mean forward scatter (FSC) was used to obtain an estimate of mean cell length by calibrating FSC against calibration beads of a known size along with 18 marine phytoplankton species of a known average length (Figure S3) (Barton & Yvon-Durocher, 2019). Following this, we could estimate cell volume (in μm^3) for each of the species (see Section 2.8).

2.3 | Specific growth rate for growth rate trajectories

Using the estimates of population density, at the beginning and end of each transfer period, we calculated specific growth rate (μ , day^{-1}) using the following equation (Wood et al., 2005):

$$\mu = \frac{\ln(N_{t1} - N_{t0})}{\Delta t} \quad (1)$$

where N_{t1} is the population density at the end of the transfer period (when cells are still in exponential phase), N_{t0} is the inoculation density and Δt is the time passed in days since the inoculation.

Approximate number of generations passed between each transfer period could then be calculated from the estimated doubling time:

$$\text{Number of generations} = \Delta t / \left(\frac{0.6931}{\mu} \right) \quad (2)$$

where $0.6931/\mu$ (or $\log(2)/\mu$) gives the calculated doubling time based on the estimated specific growth rate, μ , assuming mortality is zero, and Δt is the time passed in days since the inoculation.

2.4 | Population density and growth rate trajectories

We used the specific growth rate calculated at each transfer to track the changes in fitness of the replicates over the 22-week period (up to 27 weeks when including the time period where additional physiological data were collected). The cytometry data from each weekly transfer also allowed us to track population density during exponential growth over the duration of the experiment. Crucially, we

were interested in investigating the effect of growth temperature on these trajectories. Due to the different shape of the trajectories across the treatments, and the species, we used generalized additive mixed effects models (GAMMs) to assess the effect of the growth temperature. These were fitted to the data using the 'gam4' package in R (v4.1.2). This process was repeated for the specific growth rate trajectories of each species, along with the trajectories of exponential phase population density (see Figure 2; Figure S1; Table S2). This approach allowed us to account for the hierarchical nature of our data, whereby for each of the species at each temperature, we had six individual biological replicates with their own unique trajectory. We therefore treated replicate as a random effect on the intercept of all the models. The most complex model included the fixed effect of treatment temperature (i.e., control temperature and warmed temperature) on both the intercept (characterizing the median value of the response variable) and the shape of the time-series response (which is modelled using a cubic regression spline, to vary across the treatments). The best model was selected by computing sample size corrected Akaike information criterion scores (AICc) and then comparing these across all of the models, with the best model having the lowest AICc score that was more than 2 ΔAICc scores lower than the second best model. AICc weights also identified the strength of the best model relative to the others. These model comparisons were made using the 'MuMIn' package in R.

2.5 | Thermal tolerance curves

Following the 22-week experimental period, we remeasured the thermal tolerance curves of cultures from both control and warmed treatments for each species. This involved inoculating each biological replicate into fresh growth medium with the same starting density for each species and placing them in incubators at a range of assay temperatures from 15°C to 35°C. Daily population density measurements were made using flow cytometry for approximately 20 days (or until stationary phase was reached).

We modelled specific growth rate for each replicate at each assay temperature by log transforming the population density measurements and running linear regressions through the exponential phase of the growth data (this process meant that a mean of seven points were used to fit the linear regression across all the replicate measurements, with a minimum of 3 and a maximum of 14 points, where the smaller number of points typically represents faster growth rates and therefore fewer days over which to measure exponential growth). This was achieved through linear mixed effects modelling, using the 'lme4' package in R, whereby we included the random effect of each specific biological replicate (across all species and treatments) on both the slope and intercept of the relationship between the natural logarithm transformed population density and the number of days at the assay temperature. This returned us replicate-specific deviations of both the slope and intercept from the overall response, with the slope coefficients derived for each replicate at each assay temperature being used here as our specific

growth rate estimates (as outlined by Equation 1). In some instances where there were declines in population density that did not recover within the 20 days, we selected the linear decline in the data before running the model and thus obtained negative growth rates.

To select a suitable model for fitting the thermal tolerance curves to the specific growth rate data, we took advantage of the recent R packages 'rTPC' and 'nls.mltstart' (Padfield et al., 2021; Padfield & Matheson, 2018). This approach enabled us to fit and select the best model that can work with negative growth rates, allowing us to reliably model the extreme limits of thermal tolerance. We described differences in the thermal tolerance across species and treatments by empirically calculating various universal traits from the model fits. Our parameters of interest were r_{max}^{μ} (the maximum growth rate), T_{opt}^{μ} (optimal temperature of growth, that yields r_{max}^{μ}), T_{max}^{μ} (the maximum temperature limit of growth) and TSM (the thermal safety margin, which is the difference between T_{opt}^{μ} and T_{max}^{μ}). To make sure we used the model that best fit to our data, we did a model selection process with the five models in the 'rTPC' package that can handle negative data ('johnehk_2008', 'kamykowski_1985', 'lactin2_1995', 'thomas_2012' and 'thomas_2017'). Using 'rTPC' in conjunction with the 'nls.mltstart' package, we determined the best fit of each model to each biological replicate curve. This method applies the 'nlsLM' function in the 'minpack.lm' package and uses a modified Levenberg–Marquardt optimization algorithm, returning the model with the best AIC scores after fitting the model 1000s of times using a gridstart approach of random combinations of different starting parameter values for each model run. The 'thomas_2012' was the best model in most cases, giving the lowest AIC scores for 19 of 24 curves (see Table S3). Following model selection, we then used the returned parameters from the 'thomas_2012' model fits to obtain high-resolution predictions for all replicates to allow estimation of the thermal tolerance traits described above (see Figure 3a,f; Figure S4; Tables S4 and S5). We also obtained treatment level fits for visualization of the overall effect of the experimental treatment, by re-running the above procedure but ignoring the replicate nesting of the data to derive a set of parameters specific to the average treatment response of each species (see Figure 3a,f; Figure S5; Tables S4 and S5).

To determine whether there was a significant shift in any of the thermal tolerance traits for each species as a result of adaptation to the warmed treatment (see Figure 3b–e,g–j), we used a post hoc analysis of variance followed by a Tukey multiple comparison of means to determine the magnitude and significance of the changes in thermal tolerance curve traits across the biological replicates, this is summarized in Table S6. These shifts are also supported by the 95% confidence intervals derived from the model fitting (see Figures S4 and S5; Tables S4 and S5).

As mentioned in the experimental design section, the thermal tolerance of the pre-clonal cultures was also modelled for each of the species to identify a suitable supra-optimal temperature for our warmed treatments. We followed the same procedure as above, fitting the 'thomas_2012' model to the curves. We could only model the

thermal tolerance parameters at the level of species in this instance, as the replication of growth measurements at each assay temperature was only technical, with all inoculations coming from the same stock of each species (i.e., no biological replication). Nonetheless, from the predictions of r_{max}^{μ} and T_{opt}^{μ} , we were able to identify suitable supra-optimal treatment temperatures that gave predicted rates that were approximately 50% of r_{max}^{μ} (rounded to the nearest 1°C; see Figure 1b; Table S1).

2.6 | Estimates of carbon and nitrogen per cell

For each biological replicate, while in exponential growth, 50–100 mL of culture of known population density was aliquoted into falcon tubes and centrifuged at 3500 r.p.m at 4°C for 45 min. The pelleted cells were rinsed with deionized water and re-spun three times to remove any artificial sea water residue, and subsequently freeze-dried using a CoolSafe (95-15 PRO, ScanVac) over a 24-h period and weighed to obtain dry weight. Samples were distributed into tin cups and sent to Elementex (Elementex Ltd, Cornwall, UK, PL17 8QS) for elemental analysis of %C and %N using a SerCon Isotope Ratio Mass Spectrometer (CF-IRMS) system (continuous flow mode). For each biological replicate, we then calculated pg C cell⁻¹ (picograms of carbon per cell), pg N cell⁻¹ (picograms of nitrogen per cell) and the C:N ratio (the carbon to nitrogen ratio). Corresponding flow cytometry data were used to estimate the average cell volume for each of the replicates, as described below (see Equations 5 and 6, Figure S3; Table S7). Volume-specific concentrations of carbon and nitrogen were derived by dividing the measured per cell quota by the estimated cell volume.

2.7 | Chlorophyll *a* per cell measurements

For each biological replicate, 50 mL culture of a known population density in exponential growth was centrifuged at 3500 r.p.m, for 45 min at 4°C. The pelleted cells were re-suspended in 6 mL of ethanol (100%) by vortexing and were then refrigerated in the dark for 24 h. Following this, samples were vortexed once more and remnant cell debris was pelleted by centrifugation at 3500 r.p.m for 3 min, leaving the chlorophyll pigmented supernatant. Using a spectrophotometer (Jenway 7315), we measured the absorbance profile of the supernatant by scanning from 610 to 750 nm for three technical replicates per biological replicate. Blanks were measured across the same wavelength range to correct for the ethanol absorbance. We used well-established absorbance coefficients to obtain estimates of pg chlorophyll *a* cell⁻¹ for each of the biological replicates. Due to differences in the pigment composition across the species, different equations were used (Ritchie, 2006):

Cyanobacteria (*Synechococcus* sp.):

$$\mu\text{g chlorophyll } a \text{ cell}^{-1} = \frac{(11.9035 A_{665} - A_{730})v}{\text{cells mL}^{-1}} \quad (3)$$

Chlorophytes (*Ostreococcus tauri*):

$$\mu\text{g chlorophyll } a \text{ cell}^{-1} = \frac{(-5.2007 A_{649} + 13.5275 A_{665} - A_{730})v / (lV)}{\text{cells mL}^{-1}} \quad (4)$$

where A_{xxx} is the absorbance at xxx nm (A_{730} represents the background absorbance), v is the volume of solvent used for the extractions (in this case 6 mL of ethanol), l is the length of the spectrophotometric cell (in this case 1 cm), V is the original sample volume (in this case 50 mL) and cells mL^{-1} is the population density of the original culture in exponential growth phase (Henriques et al., 2007; Ritchie, 2006) (see Figure 5; Table S7). Volume-specific concentrations of chlorophyll a were derived by dividing the measured per cell quota by the estimated cell volume (see Figure 6).

2.8 | FSC conversion factor and cell volume calculation

As described above, we calibrated cytometry FSC values against beads and species of a known length. This allowed us to derive the following conversion factor (see Figure S3):

$$\ln \text{ cell length } (\mu\text{m}) = (0.57 \times \ln \text{FSC}) - 5.93 \quad (5)$$

where cell length is measured in μm , and FSC represents mean forward scatter measured by the flow cytometry. Assuming a spherical geometry, we then used the following equation to derive cell volume of the species at the time of per cell carbon, nitrogen and chlorophyll a measurements (Hillebrand et al., 1999; Sun & Liu, 2003):

$$\text{cell volume } (\mu\text{m}^3) = \frac{\pi}{6} \times \text{cell length } (\mu\text{m})^3 \quad (6)$$

2.9 | Principal components analysis

Variance in different functional traits across the species and treatments was examined using principal component analysis (PCA), this was conducted using the 'prcomp' function in the 'stats' package in R. This analysis was performed on the following traits: estimated cell volume, pg C cell^{-1} , pg N cell^{-1} , $\text{pg chlorophyll } a \text{ cell}^{-1}$, C:N, r_{max} , T_{opt} and T_{max} .

The first two principal components, which combined accounted for >85% of the total variance, were used to define the axes of the plot onto which results were projected. Loadings scores for each of the variables were derived and plotted on the same axis to demonstrate any possible negative or positive covariance of the traits. Ellipses were plotted as a visual guide to the clustering of the different treatment replicates and reflect 95% confidence intervals around the centroid of each cluster giving us an indication of whether the treatment replicates can be uniquely identified by the traits included in the PCA (see Figure 4; Table S10). For all of the traits included in the PCA, we also used a post hoc analysis of variance followed by a Tukey multiple comparison of means to determine any significant

effect of treatment on the measured values (see Tables S6 and S8).

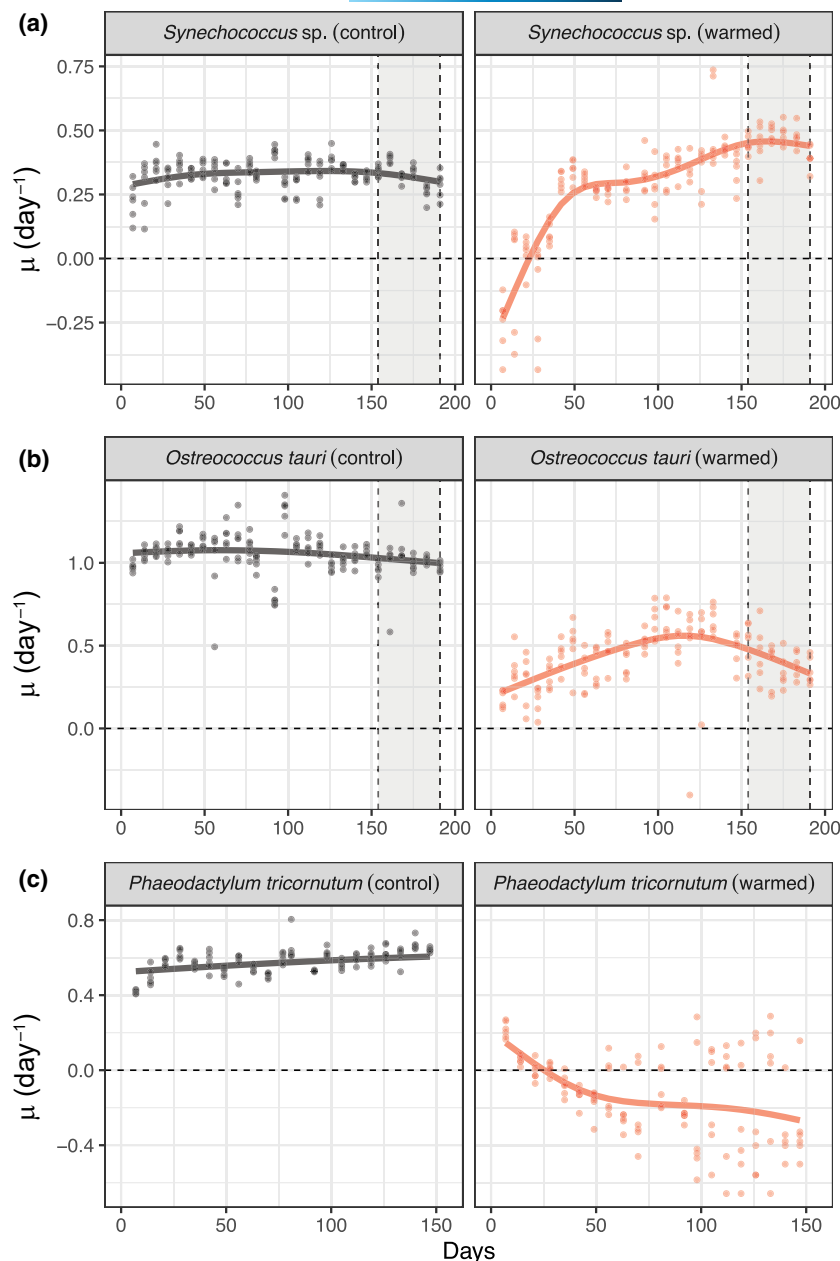
3 | RESULTS

3.1 | Patterns of adaptation in long-term fitness tracking

To investigate the relative capacity of different phytoplankton species to adapt to warming, we applied standardized long-term experiments simultaneously across three phylogenetically diverse marine phytoplankton species. We determined supra-optimal temperatures for each species where measured growth rates of stock populations were reduced to ~50% of their maximal performance at T_{opt} (see Figure 1b; Table S1), we then exposed six clonal populations of each species to both the control temperature and supra-optimal temperature for the same length of time (22 weeks). This enabled us to monitor the relative changes in fitness (or growth rate) of each species population over the experimental period.

Across all species, our GAMM analysis (see Section 2.4) found that there was a significant effect of experimental treatment on both the intercept and shape of the growth rate trajectories relative to the control, and this was mirrored by changes in population density at the point of each weekly transfer (see Figure 2; Figure S1; Table S2). Initially, *Synechococcus* sp. had negative growth rates for the first 2–3 weeks, but following this their growth rates and population density at each transfer rapidly increased. They reached comparable growth rates to the control treatment within 50 days, and eventually exceeded the growth rates of the control by twofold by the end of the experiment ($\sim 0.5 \text{ day}^{-1}$), having passed a similar total number of ~90 generations (see Figure 2a; Figures S1 and S2a). All replicates of *Ostreococcus tauri* maintained positive specific growth rates in response to the warmed treatment, increasing to a maximum of $\sim 0.5 \text{ day}^{-1}$ over the first half of the experiment, but growth rates remained lower than the control throughout. After ~110 days, growth rates then gradually declined, reaching $\sim 0.3 \text{ day}^{-1}$ by the end of the experimental period (see Figure 2b). This is reflected by almost three times as many total generations passing in the control (~300 generations) relative to the warmed treatment (~115 generations, see Figure S2b). In contrast, abundances and growth rates of *Phaeodactylum tricornutum* declined consistently following the initial inoculations (see Figure 2c; Figure S1). While it was possible to measure positive growth rates at the control temperature, the continuous decline in population density in response to the warmed treatment meant that we measured negative growth rates for the majority of the experimental period, and thus, no weekly transfers were made. There was some indication of a few replicates showing positive growth towards the latter stages, but this was not sustained and did not result in a recovery of any replicate populations, with cell numbers ~2 orders of magnitude lower than the initial starting density (see Figure S1). Therefore, we conclude that in comparison to the other two species, *Phaeodactylum tricornutum* was unable to adapt over the 22-week duration of the experiment. Furthermore, due

FIGURE 2 Growth rate trajectories for (a) *Synechococcus* sp., (b) *Ostreococcus tauri* and (c) *Phaeodactylum tricornutum* at each of their respective treatment temperatures. Data points represent specific growth rate measurements for the six biological replicates at each treatment temperature, and the fitted line for each of the treatments represents the best fits of the selected GAMM for each of the species (see Section 2.4). Plots on the left present the changes in growth rate at the control temperature (in black). Plots on the right present the changes in growth rate at the warmed temperature treatment (in red). The first of the dashed vertical lines highlight the end of the 22-week experimental period, and the shaded area represents the 5-week period during which all other physiological data were collected, up to the second vertical dashed line at the 27-week mark. *Phaeodactylum tricornutum* demonstrated continuous decline in growth rate and population size (see Figure S1) and this made it unfeasible to collect any additional physiological data at the end of the experimental period for this species (hence no shaded region between the 22- and 27-week marks).



to the very low population densities and poor health of the warmed replicates by the end of the experimental period, this meant that we were unable to collect any complimentary physiological data sets for these replicates.

3.2 | Shifts in thermal tolerance following thermal adaptation

Following the 22-week experimental period, to further explore how the observed improvement in fitness (in response to the supra-optimal treatment) were reflected in changes to thermal tolerance of both *Synechococcus* sp. and *Ostreococcus tauri*, we remeasured the thermal tolerance curves of both the control and warmed treatment replicates (see Section 2.5, and Figure 3a–j; Tables S4 and S5).

We observed a significant shift in the tolerance curves of both species (see Table S6 for summary of post hoc analysis of variance). At the control temperature, *Ostreococcus tauri* replicates had an average T_{opt}^{μ} and T_{max}^{μ} (the maximum temperature limit of growth) of 27.0°C (95% CI: 26.67–27.55) and 36.3°C (95% CI: 35.85–36.56). These respective traits increased to 28.9°C (95% CI: 27.76–29.11) and 37.6°C (95% CI: 36.93–38.09) for the high-temperature evolved strains. This resulted in a non-significant narrowing of the average thermal safety margin (TSM), which is the difference between T_{opt}^{μ} and T_{max}^{μ} , by ~0.5°C. In combination with a raised T_{opt}^{μ} , the warmed replicates also demonstrated a significant reduction in maximal growth rates at the optimal temperature, r_{max}^{μ} , by approximately 12.5% (see Table S4). *Synechococcus* sp. had an average control T_{opt}^{μ} and T_{max}^{μ} of 24.9°C (95% CI: 24.61–25.12) and 28.3°C (95% CI: 28.14–28.41), and an average warmed T_{opt}^{μ} and T_{max}^{μ} of 27.2°C (95%

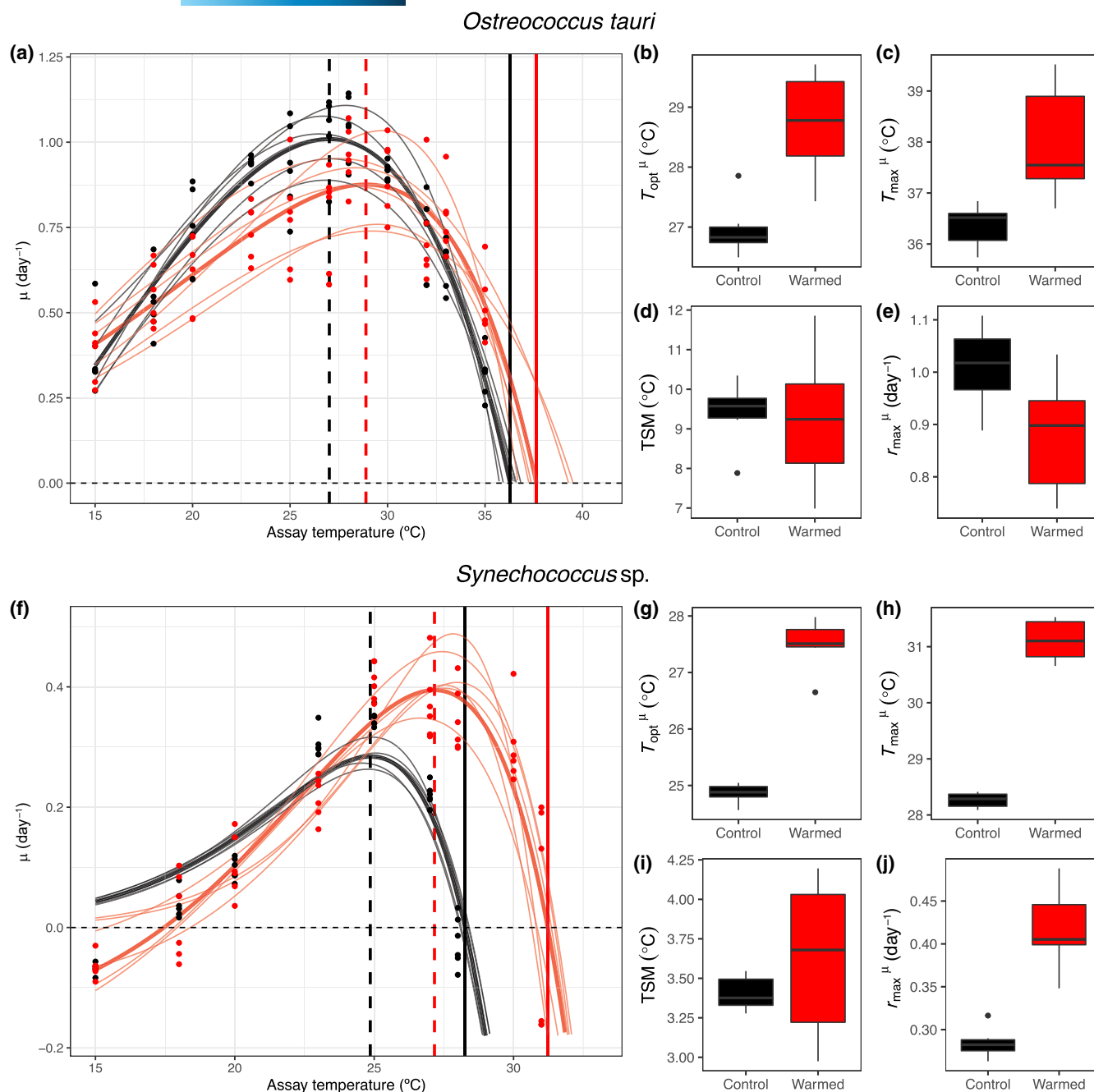


FIGURE 3 Thermal tolerance curves and the modelled parameters for both the control and warmed treatment replicates of *Ostreococcus tauri* (a–e) and *Synechococcus* sp. (f–j). Black colouring denotes control treatment data, and red denotes the warmed treatment data. Data points represent the measured specific growth rate of each biological replicate in response to each assay temperature. For each biological replicate (fine curves), model fits were derived from the ‘thomas_2012’ model using the ‘rTPC’ R package (as described in the Section 2.5). For visualization purposes, model fits were also derived for the average growth rate responses for each treatment (bold curves). The dashed vertical line corresponds to the average T_{opt}^{μ} value, and the bold vertical line the average T_{max}^{μ} (the maximum temperature limit of growth). The box and whisker plots for each of the species illustrate the resultant divergences in the thermal tolerance parameters following approximately 22 weeks at each treatment, where TSM is the thermal safety margin (which is the difference between T_{opt}^{μ} and T_{max}^{μ}) and r_{max}^{μ} (the maximum growth rate). All shifts in parameters were significant for both species, except for the TSM (see Table S6). In (b–e) and (g–j), tops and bottoms of the bars represent the 75th and 25th percentiles of the data, the horizontal lines are the medians and the whiskers extend from their respective hinge to the smallest or largest value no further than $1.5 \times$ interquartile range (distributions are made of six data points representing each biological replicate, see Tables S4 and S5).

CI: 26.39–27.73) and 31.2°C (95% CI: 30.88–31.48) respectively. This demonstrated a non-significant increase in the average TSM by $\sim 0.6^\circ\text{C}$ as a result of adaptation to the warmed treatment. In contrast to the response of *Ostreococcus tauri*, there was a significant increase in r_{\max}^μ in response to the warmed treatment by approximately 30% (see Table S5).

These results are consistent with the fitness trajectory data (see Figure 2), whereby in the response to the warmed treatment, *Synechococcus* sp. showed an increase in growth rates beyond the control, whereas *Ostreococcus tauri* sustained growth rates that were lower than the control. The differing changes to the thermal tolerance curves across the two species support recent work that has shown that phytoplankton thermal adaptation does not necessarily follow strong thermodynamic constraints (Barton & Yvon-Durocher, 2019; Kontopoulos et al., 2020; Liu et al., 2022), that is, we do not always associate higher thermal optima (T_{opt}^μ) with greater maximal rates (r_{\max}^μ), as may be expected from the 'hotter-is-better'

hypothesis—which is often the common assumption in modelling based studies that apply the 'Eppley' coefficient to determine phytoplankton productivity responses to warming (Eppley, 1972; Laufkotter et al., 2015; Stock et al., 2014). While the effect of long-term warming on absolute magnitude of growth rates is different across the two species, what is consistent is an overall shift in the thermal safety margin to a higher temperature range in both cases (characterized by an increase in both T_{opt}^μ and T_{\max}^μ). On this note, although *Ostreococcus tauri* did not elevate r_{\max}^μ as an adaptive response to warming, it did maintain a much wider TSM in comparison to *Synechococcus* sp. (average TSMs of 8.74°C and 4.06°C, for *Ostreococcus tauri* and *Synechococcus* sp., respectively, in response to warmed treatment; see Tables S4 and S5), as was also observed in the control responses and the pre-clonal thermal tolerance curves (see Figure 1b). This indicates that despite *Synechococcus* sp. showing the greater potential to adapt and improve fitness (increasing its TSM and r_{\max}^μ), it is still more vulnerable relative to *Ostreococcus*

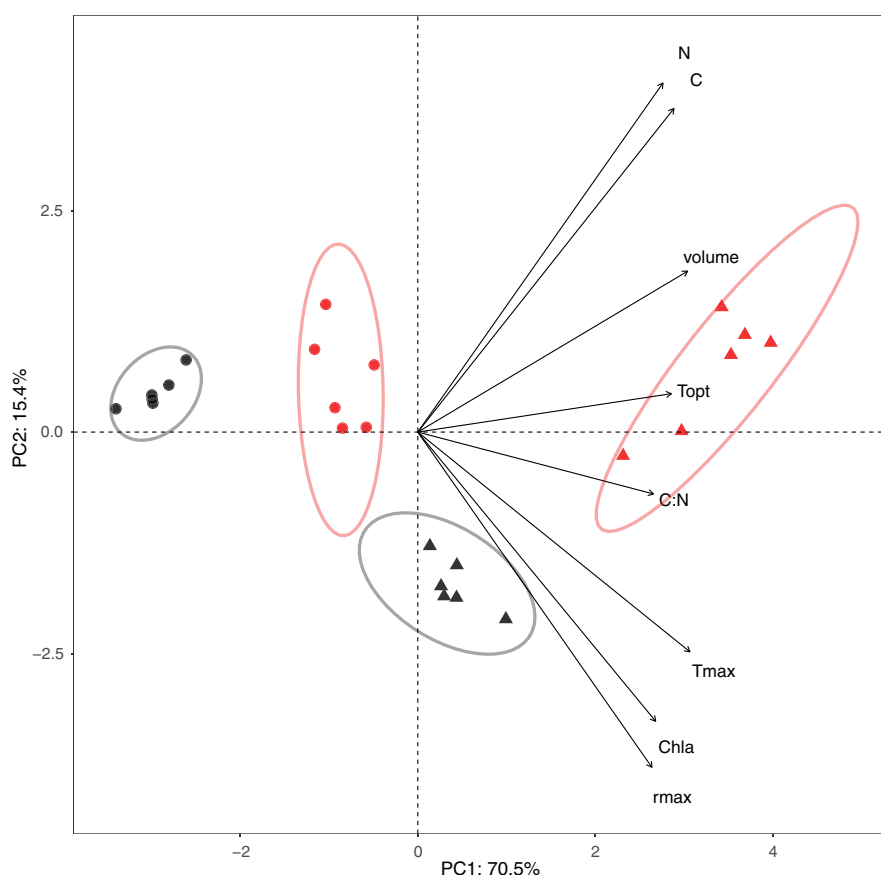


FIGURE 4 Principal component analysis of the trait data for each of the control and warm-adapted replicates of both *Ostreococcus tauri* and *Synechococcus* sp. Triangles denote *Ostreococcus tauri* biological replicates, and circles denote *Synechococcus* sp. biological replicates, with black and red colouring denoting control and warmed treatments respectively. The axes are derived from the first two principal components and make up >85% of the total variance in the data. The loadings for each of the variables included in the analysis are plotted to demonstrate the correlations and covariance of traits (see Table S10), where volume = estimated cell volume, T_{opt} = optimal growth temperature (T_{opt}^μ), T_{max} = maximum growth temperature (T_{max}^μ), r_{\max} = maximal growth rate (r_{\max}^μ), C:N = C:N ratio, C = pg C cell⁻¹, N = pg N cell⁻¹ and Chla = pg chlorophyll a cell⁻¹. The length of each loading vector reflects the combined weighting of each variable in the first two principal components; these lengths were multiplied by a constant for visualization purposes. Ellipses were plotted as a visual guide to the clustering of the different treatment replicates and reflect 95% confidence intervals around the centroid of each cluster giving us an indication of whether the treatment replicates can be uniquely identified by the traits included in the PCA (for boxplots of these traits, see Figures 3, 5 and 6).

tauri in terms of the absolute range of temperatures it can tolerate beyond its thermal optima. This provides an interesting comparison about potential adaptive trade-offs, where on the one hand, *Synechococcus* sp. may be able to outcompete others by increasing its maximal performance, and on the other hand, *Ostreococcus tauri* has the advantage of being able to tolerate a wider range of temperatures beyond its thermal optimum.

3.3 | Cellular trait trade-offs

Next, to determine how thermal adaptation may impact the biogeochemical function of each species, we used a PCA to investigate how shifts in thermal tolerance correlate with biochemical traits (see Section 2.9 and Figure 4). We then used a simple post hoc analysis of variance to further explore the significance of some of the trait shifts (see Tables S8 and S9), this is also presented graphically (see Figures 5 and 6).

Our PCA illustrates clear differentiation between the warm-adapted replicates and the control replicates for each of the species, and demonstrates that the shifts in traits associated with cell size (cell quotas of carbon, nitrogen and chlorophyll *a*) are positively correlated with shifts to higher thermal tolerance. Both *Ostreococcus tauri* (~4 fold) and *Synechococcus* sp. (~3-fold) increased in cell volume following long-term exposure to stressful high temperatures

(see Figure 6; Tables S7 and S8). This finding is contradictory to the generally expected temperature size rule which predicts a negative effect of warmer environments on size (Atkinson, 1995; Atkinson & Sibly, 1997), but in agreement with some previous studies that have found that experimental warming resulted in increased cell size of the diatom *Thalassiosira pseudonana* (Schaum et al., 2018; Sheehan et al., 2020) and a doubling in cell size of the cyanobacteria *Prochlorococcus* (Fu et al., 2007). Specifically in relation to supra-optimal warming, it has also been shown in two species of diatom that, where growth rates are reduced due to high-temperature stress, cell volume increases (Anderson & Ryneearson, 2020).

In the case of *Synechococcus* sp., we found an ~3-fold increase in chlorophyll *a* content per cell in the warm-adapted replicates, but in *Ostreococcus tauri*, there was no significant change relative to the control (see Figure 5). A number of previous studies have also found an increase in per capita chlorophyll *a* in warm-adapted phytoplankton cultures (Baker et al., 2018; Schaum et al., 2017; Sheehan et al., 2020), and similar to our result for *Synechococcus* sp., this has been linked to greater fitness relative to ambient adapted isolates (Schaum et al., 2017). It is worth highlighting that when per cell quotas were converted to volume-specific concentrations, there was no effect of warm adaptation on the chlorophyll *a* concentration in *Synechococcus* sp., whereas in *Ostreococcus tauri*, we see a statistically significant decrease in chlorophyll *a* concentration (see Figure 6; Table S9). This suggests

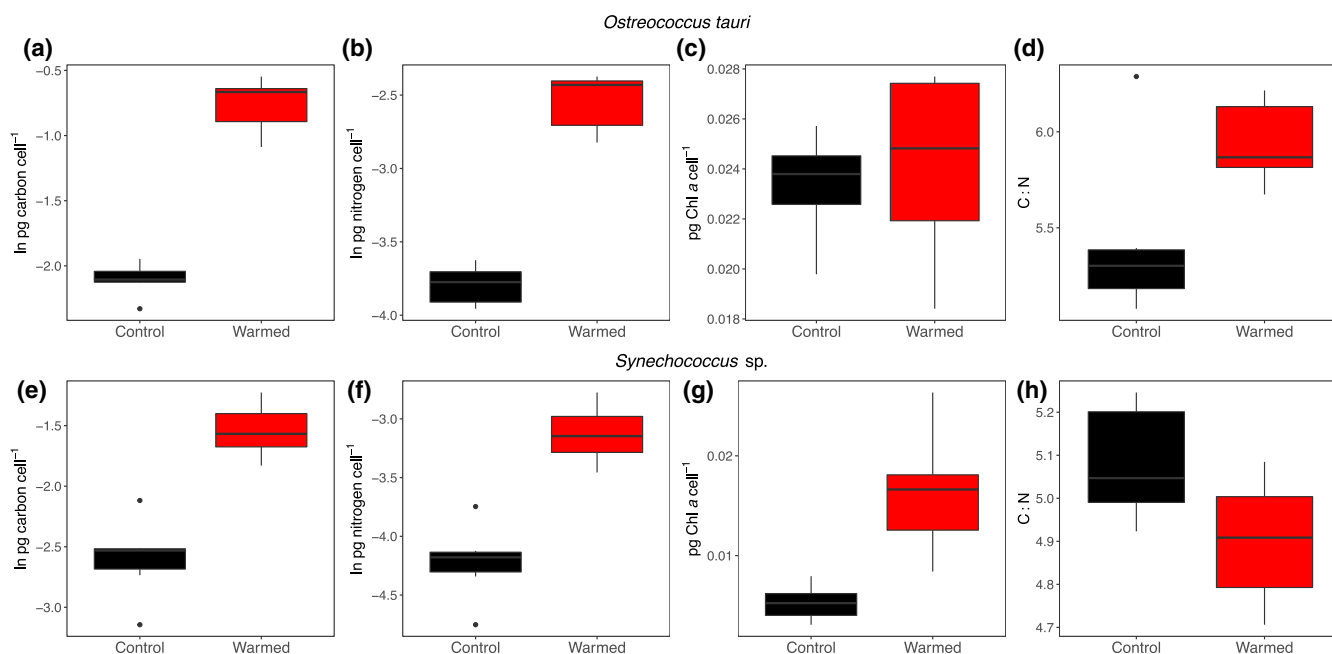


FIGURE 5 Cellular biochemical trait differences between the control and warm-adapted treatment replicates of both *Ostreococcus tauri* (a–d) and *Synechococcus* sp. (e–h). For both species, there was a significant increase in carbon and nitrogen content per cell in the warm-adapted replicates (a, b, e, f). There was a significant increase in the C:N ratio of the warmed replicates of *Ostreococcus tauri* (d), but for *Synechococcus* sp., there was a decrease in the C:N ratio (h). Chlorophyll *a* content per cell increased in the warm-adapted *Synechococcus* (g), but for *Ostreococcus*, there was no significant difference with the control replicates (c). Tests for significant differences in the traits displayed in this figure are summarized in Table S8, with all being significant except for chlorophyll *a* in *Ostreococcus tauri*. Values of both nitrogen and carbon content per cell are natural log transformed for visualisation purposes. Boxplots distributions are made of six data points representing each biological replicate, see Figure 3 for a guide to the aesthetics.

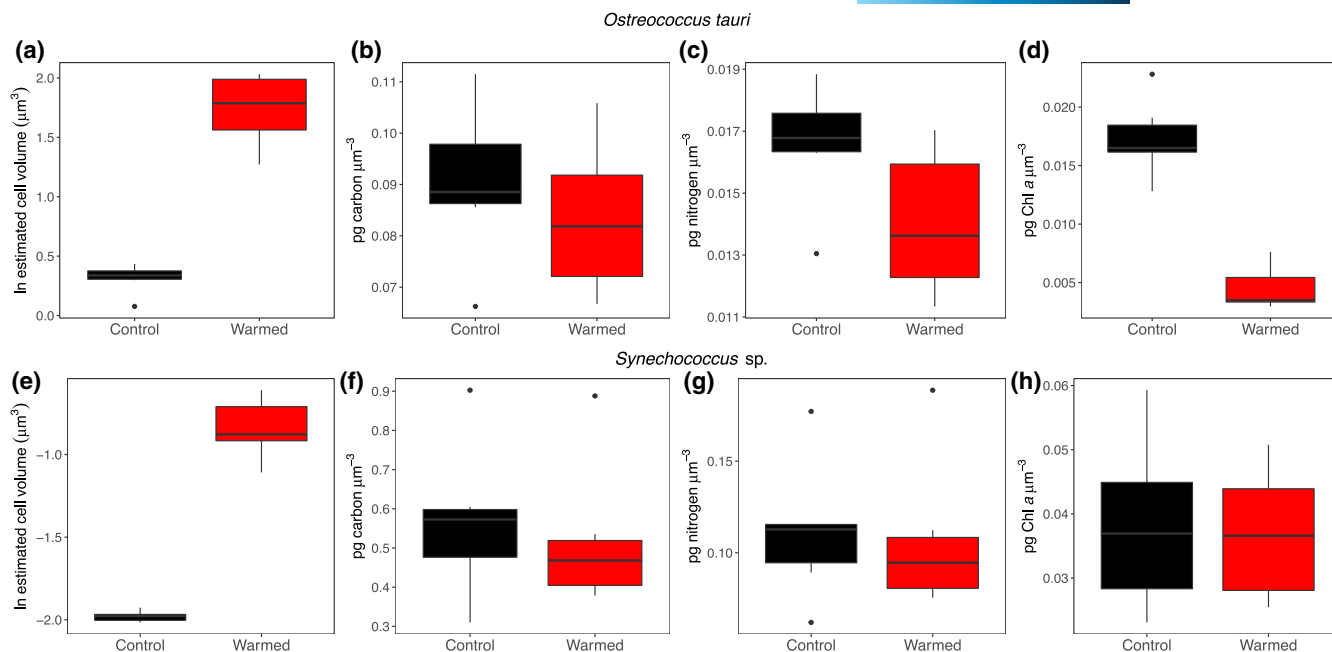


FIGURE 6 Volume-specific biochemical trait differences between the control and warm-adapted treatment replicates of both *Ostreococcus tauri* (a–d) and *Synechococcus* sp. (e–h). For both species, there is a significant increase in estimated cell volume in the warm-adapted replicates (a, e). There is no effect of treatment on carbon concentration (b, f) and nitrogen concentration for either species (c, g), though this is marginal for *Ostreococcus tauri*, where there appears to be an overall decrease in the concentration of nitrogen ($p = .07$). There is a significant decrease in the chlorophyll *a* concentration in warm-adapted *Ostreococcus tauri* (d), but there is no effect of treatment on the chlorophyll *a* concentration in *Synechococcus* sp. (h). Tests for significant differences in traits displayed in this figure are summarized in [Tables S8](#) and [S9](#). Values of estimated cell volume are natural log transformed for visualization purposes. Boxplots distributions are made of six data points representing each biological replicate, see [Figure 3](#) for a guide to the aesthetics.

that despite the overall increases in cell volume observed in both species as an adaptive response, *Synechococcus* sp. retained the same volume-specific concentrations of chlorophyll *a*, whereas *Ostreococcus tauri* was unable to increase chlorophyll *a* concentrations proportionally with size.

Of wider biogeochemical relevance, and in line with the increase in cell size of both *Ostreococcus tauri* and *Synechococcus* sp., we also measured an increase in per cell content of carbon and nitrogen (both of which increased by ~3- to 4-fold for each species, see [Figure 5](#)). When these values were converted to volume-specific concentrations, there was no significant effect of warm adaptation on the concentrations of carbon and nitrogen in *Synechococcus* sp.; however in warm-adapted *Ostreococcus tauri*, there was an almost significant decrease in the concentration of nitrogen (see [Figure 6](#); [Table S9](#)). The lower concentrations of both nitrogen and chlorophyll *a* in warm-adapted *Ostreococcus tauri*, which are likely to be tightly coupled (Evans, 1989), could help to explain the significantly greater carbon to nitrogen ratio (C:N) relative to the control (see [Figures 5](#) and [6](#); [Tables S8](#) and [S9](#)). We can speculate that the observed decrease in chlorophyll *a* and nitrogen concentrations is consequently linked to reduced productivity, and reflected in the lower overall growth rates in the warm-adapted replicates of *Ostreococcus tauri*. The lower C:N in the warm-adapted *Synechococcus* sp. relative to the control (see [Figure 5](#); [Table S8](#)) might be reflected in the observed temperature

enhanced growth rates. Indeed, previous work on eukaryotic phytoplankton has predicted an increase in cellular nitrogen demands with warming is likely to be a consequence of enhanced ribosomal function and protein synthesis at higher temperatures, thus bringing down C:N (Toseland et al., 2013). More generally, the lower C:N values for *Synechococcus* sp., relative to *Ostreococcus tauri*, are expected because smaller phytoplankton cell types are associated with reduced carbon storage, as well as greater relative abundance of nitrogen containing molecules associated with non-scalable cellular components, such as nucleic acids and membrane proteins (Marañón et al., 2013; Raven, 1994). Overall, regardless of whether increase in nitrogen quota is driven simply by increase in cell size (as seen for both *Synechococcus* sp. and *Ostreococcus tauri*) and/or increased cellular demand for protein synthesis (speculatively suggested here for *Synechococcus* sp.), if such adaptive shifts were to emerge in natural populations, the increase in per-capita stoichiometric demands of nitrogen would inevitably have implications for nutrient availability and marine communities as a whole.

4 | DISCUSSION

Our standardized experiments allowed us to explore the relative capacity for thermal adaption across a diverse range of marine phytoplankton species. In doing so, our results demonstrate a striking

pattern. The largest and most complex organism, *Phaeodactylum tricornutum* (Bowler et al., 2008) failed to adapt. The second largest species, *Ostreococcus tauri* (albeit the smallest known eukaryote: Courties et al., 1994; Derelle et al., 2006; Palenik et al., 2007), did adapt but failed to attain growth rates that were comparable to those observed at its ancestral temperature. Finally, the smallest and arguably simplest of the species *Synechococcus* sp. (Palenik et al., 2003) showed the strongest thermal adaptation in the set time period, reaching growth rates that were higher than at its ancestral temperature. These findings support theory that more complex organisms, with a larger genome size, are likely to have slower rates of adaptation (Lynch et al., 2003; Orr, 2000). Indeed, it is also plausible to suggest from our results, when directly comparing the response of *Ostreococcus tauri* and *Synechococcus* sp., that prokaryotic picophytoplankton demonstrate greater capacity to adapt and increase fitness than eukaryotic picophytoplankton. This is reflected in the lower number of generations passed for *Synechococcus* sp. (~90 generations) relative to *Ostreococcus tauri* (~115 generations), in response to their respective warmed treatments over the same time period (see Figure S2). As we started from clonal isolates, the probability that beneficial mutations would arise in the smaller species was likely to be higher given the greater attainable population sizes of both *Synechococcus* sp. and *Ostreococcus tauri* (Bell & Gonzalez, 2009; Ramsayer et al., 2013; Samani & Bell, 2010; Willi et al., 2006). It is important to note, however, that by initiating the experiment with clonal isolates, it is likely that we are underestimating adaptive potential, and had we started with non-clonal stock populations, with greater genetic diversity, we might have observed more rapid adaptive responses. Furthermore, though there is some uncertainty around possible sexual reproduction in both *Ostreococcus* (Benites et al., 2021; Grimsley et al., 2010; Leconte et al., 2020) and *Phaeodactylum tricornutum* (Mao et al., 2020), it is likely to be rare, and therefore, we should not need to consider this a factor in the relative pace and magnitude of adaptation observed. Nonetheless, if sexual reproduction had taken place, then this would not implicate the findings presented here, as it would be intrinsic to the adaptive capacity that is inferred from the standardized experimental design. Critically, if these findings do indicate a greater adaptive capacity of smaller and less complex species relative to larger species in response to warming, then this further supports previous suggestions that picophytoplankton, and perhaps cyanobacteria in particular, will be more successful in warming oceans (Anderson et al., 2021; Morán et al., 2010). This is already expected to occur where nutrient limitation at shallower depths, due to increased ocean stratification (Behrenfeld et al., 2006; Bopp et al., 2005; Duarte et al., 2013; Falkowski et al., 1998; Irwin & Oliver, 2009), will favour the prevalence of picophytoplankton due to their greater nutrient affinity (Dutkiewicz et al., 2013; Litchman & Klausmeier, 2008; Raven, 1998). A shift to phytoplankton communities dominated by picophytoplankton (such as cyanobacteria and prasinophytes) would inevitably have implications for biogeochemical cycles, in particular the biological carbon pump (Morán et al., 2010) due to decreased sinking velocities relative to 'marine snow' forming diatoms and CaCO_3 ballasted coccolithophores.

Most marine picophytoplankton are not typically bloom forming, as opposed to larger and more complex taxa (e.g., diatoms, dinoflagellates and coccolithophores). Given the fact they are widespread throughout the ocean and present all year round (Buitenhuis et al., 2012; Flombaum et al., 2020; Visintini et al., 2021; Zhong et al., 2020), their ability to rapidly adapt to warming under nutrient replete conditions (as demonstrated in the experiments presented here) could mean they have potential to outperform, or indeed replace, larger bloom forming taxa under future warming scenarios in more coastal regions or during episodic phases of high nutrient availability. This could influence trends in expected bloom formation and have knock-on ecological implications for biodiverse coastal areas. On this note however, given that nutrient-poor oligotrophic zones are expected to expand under future warming scenarios (Duarte et al., 2013; Irwin & Oliver, 2009), future work should consider varying adaptive capacity under nutrient limitation. Some studies have demonstrated that nutrient limitation can reduce thermal tolerance of phytoplankton (Andrew et al., 2019; Bestion et al., 2018; Boyd, 2019; Thomas et al., 2017) and furthermore that nutrient limitation can significantly inhibit thermal adaptation of diatoms (Aranguren-Gassis et al., 2019). Our finding of a higher per cell demand for nitrogen associated with more successful thermal adaptation could implicate the ability to adapt when nutrients are already scarce. It would therefore be of great value for long-term warming studies to be conducted on a wider range of taxa under standardized experimental conditions (as in this study), but which assess adaptive responses over multistressor gradients of both temperature and nutrient concentration (Collins et al., 2022; Litchman & Thomas, 2023; Reusch & Boyd, 2013).

5 | CONCLUSION

Up until now, while previous experimental evolution studies have been highly insightful for understanding thermal adaptation of single species, their nuanced experimental designs make it challenging to draw comparisons about relative capacity to adapt across different taxa. We have shown that a standardized experimental design allowed us to demonstrate clear differences in the ability of different phytoplankton taxa to adapt to similar levels of supra-optimal thermal stress over the same period of time. *Synechococcus* sp. responded with a significant improvement in fitness and thermal tolerance, *Ostreococcus tauri* was able to increase thermal tolerance but not improve fitness to a level that was comparable to the control treatment, and *Phaeodactylum tricornutum* was unable to adapt. Taking forward such an approach in experimental evolution studies can allow future warming-based predictions to be built upon, in relation to how diverse phytoplankton communities may be restructured when capacity to adapt is factored for, and consequently the ecological and biogeochemical implications that will arise due to the differing adaptive capacities across phylogenetic groups. In the case of our study, the results would imply that cyanobacteria (and perhaps more

broadly, picophytoplankton) may have greater capacity to adapt to a similar level of supra-optimal thermal stress relative to other taxonomic groups of phytoplankton. Turnover of communities to a composition that reflects great prevalence of picophytoplankton, in response to high levels of thermal stress, could consequently have considerable impacts for biogeochemical cycles, and notably the biological carbon pump.

AUTHOR CONTRIBUTIONS

Samuel Barton and Gabriel Yvon-Durocher conceived the study. Samuel Barton, Gabriel Yvon-Durocher and Angus Buckling designed the experimental work. Samuel Barton and Abigail Masterson conducted the experimental work. Samuel Barton, Gabriel Yvon-Durocher and Daniel Padfield analysed the data. Samuel Barton wrote the manuscript and Gabriel Yvon-Durocher, Daniel Padfield, Angus Buckling and Nicholas Smirnov contributed to revisions.

ACKNOWLEDGMENTS

This study was supported by a grant from the Leverhulme Trust (RPG-2013-335) awarded to G.Y.-D., A.B. and N.S. The authors thank Ruth Warfield for assistance with long-term culture maintenance.

CONFLICT OF INTEREST STATEMENT

The authors have no conflicts of interest to declare.

DATA AVAILABILITY STATEMENT

The data that support the findings of this study are openly available in figshare at: <http://doi.org/10.6084/m9.figshare.22100018>

ORCID

Samuel Barton  <https://orcid.org/0000-0003-2551-4297>

Daniel Padfield  <https://orcid.org/0000-0001-6799-9670>

Angus Buckling  <https://orcid.org/0000-0003-1170-4604>

Nicholas Smirnov  <https://orcid.org/0000-0001-5630-5602>

Gabriel Yvon-Durocher  <https://orcid.org/0000-0002-1749-3417>

REFERENCES

- Anderson, S. I., Barton, A. D., Clayton, S., Dutkiewicz, S., & Rynearson, T. A. (2021). Marine phytoplankton functional types exhibit diverse responses to thermal change. *Nature Communications*, 12, 6413. <https://doi.org/10.1038/s41467-021-26651-8>
- Anderson, S. I., & Rynearson, T. A. (2020). Variability approaching the thermal limits can drive diatom community dynamics. *Limnology and Oceanography*, 65, 1961–1973. <https://doi.org/10.1002/lno.11430>
- Andrew, S. M., Morell, H. T., Strzepek, R. F., Boyd, P. W., & Ellwood, M. J. (2019). Iron availability influences the tolerance of Southern Ocean phytoplankton to warming and elevated irradiance. *Frontiers in Marine Science*, 6, 1–12. <https://doi.org/10.3389/fmars.2019.00681>
- Aranguren-Gassis, M., Kremer, C. T., Klausmeier, C. A., & Litchman, E. (2019). Nitrogen limitation inhibits marine diatom adaptation to high temperatures. *Ecology Letters*, 22, 1860–1869. <https://doi.org/10.1111/ele.13378>
- Atkinson, D. (1995). Effects of temperature on the size of aquatic ectotherms: Exceptions to the general rule. *Journal of Thermal Biology*, 20(1–2), 61–74. [https://doi.org/10.1016/0306-4565\(94\)00028-H](https://doi.org/10.1016/0306-4565(94)00028-H)
- Atkinson, D., & Sibly, R. M. (1997). Why are organisms usually bigger in colder environments? Making sense of a life history puzzle. *Trends in Ecology and Evolution*, 12(2), 235–239. [https://doi.org/10.1016/S0169-5347\(97\)01058-6](https://doi.org/10.1016/S0169-5347(97)01058-6)
- Baker, K. G., & Geider, R. J. (2021). Phytoplankton mortality in a changing thermal seascape. *Global Change Biology*, 27(June), 5253–5261. <https://doi.org/10.1111/gcb.15772>
- Baker, K. G., Radford, D. T., Evenhuis, C., Kuzhiumparam, U., Ralph, P. J., & Doblin, M. A. (2018). Thermal niche evolution of functional traits in a tropical marine phototroph. *Journal of Phycology*, 54(6), 799–810. <https://doi.org/10.1111/jpy.12759>
- Barton, S., & Yvon-Durocher, G. (2019). Quantifying the temperature dependence of growth rate in marine phytoplankton within and across species. *Limnology and Oceanography*, 64(5), 2081–2091. <https://doi.org/10.1002/lno.11170>
- Behrenfeld, M. J., O'Malley, R. T., Siegel, D. A., McClain, C. R., Sarmiento, J. L., Feldman, G. C., Milligan, A. J., Falkowski, P. G., Letelier, R. M., & Boss, E. S. (2006). Climate-driven trends in contemporary ocean productivity. *Nature*, 444, 752–755. <https://doi.org/10.1038/nature05317>
- Bell, G., & Gonzalez, A. (2009). Evolutionary rescue can prevent extinction following environmental change. *Ecology Letters*, 12, 942–948. <https://doi.org/10.1111/j.1461-0248.2009.01350.x>
- Benites, L. F., Buchini, F., Sanchez-Brosseau, S., Grimsley, N., Vandepoele, K., & Piganeau, G. (2021). Evolutionary genomics of sex-related chromosomes at the base of the green lineage. *Genome Biology and Evolution*, 13, 1–16. <https://doi.org/10.1093/gbe/evab216>
- Bestion, E., Barton, S., García, F. C., Warfield, R., & Yvon-Durocher, G. (2020). Abrupt declines in marine phytoplankton production driven by warming and biodiversity loss in a microcosm experiment. *Ecology Letters*, 23, 457–466. <https://doi.org/10.1111/ele.13444>
- Bestion, E., Schaum, C.-E., & Yvon-Durocher, G. (2018). Nutrient limitation constrains thermal tolerance in freshwater phytoplankton. *Limnology and Oceanography Letters*, 3, 436–443. <https://doi.org/10.1002/lol2.10096>
- Bopp, L., Aumont, O., Cadule, P., Alvain, S., & Gehlen, M. (2005). Response of diatoms distribution to global warming and potential implications: A global model study. *Geophysical Research Letters*, 32, 1–4. <https://doi.org/10.1029/2005GL023653>
- Bowler, C., Allen, A. E., Badger, J. H., Grimwood, J., Jabbari, K., Kuo, A., Maheswari, U., Martens, C., Maumus, F., Otilar, R. P., Rayko, E., Salamov, A., Vandepoele, K., Beszteri, B., Gruber, A., Heijde, M., Katinka, M., Mock, T., Valentin, K., ... Grigoriev, I. V. (2008). The *Phaeodactylum* genome reveals the evolutionary history of diatom genomes. *Nature*, 456, 239–244. <https://doi.org/10.1038/nature07410>
- Boyd, P. W. (2019). Physiology and iron modulate diverse responses of diatoms to a warming Southern Ocean. *Nature Climate Change*, 9, 148–152. <https://doi.org/10.1038/s41558-018-0389-1>
- Buitenhuis, E. T., Li, W. K. W., Vaulot, D., Lomas, M. W., Landry, M. R., Partensky, F., Karl, D. M., Ulloa, O., Campbell, L., Jacquet, S., Lantoin, F., Chavez, F., MacIsaac, D., Gosselin, M., & McManus, G. B. (2012). Picophytoplankton biomass distribution in the global ocean. *Earth System Science Data*, 4, 37–46. <https://doi.org/10.5194/essd-4-37-2012>
- Cheng, L., Zhang, S., Xie, Z., Li, D., Lin, L., Wang, M., & Wang, D. (2022). Metabolic adaptation of a globally important diatom following 700 generations of selection under a warmer temperature. *Environmental Science and Technology*, 56(8), 5247–5255. <https://doi.org/10.1021/acs.est.1c08584>
- Collins, S., Whittaker, H., & Thomas, M. K. (2022). The need for unrealistic experiments in global change biology. *Current Opinion in Microbiology*, 68, 102151. <https://doi.org/10.1016/j.mib.2022.102151>
- Courties, C., Vaquer, A., Troussellier, M., Lautier, J., Chretiennot-Dinet, M. J., Neveux, J., Machado, C., & Claustre, H. (1994).

- Smallest eukaryotic organism. *Nature*, 370, 255. <https://doi.org/10.1038/370255a0>
- Derelle, E., Ferraz, C., Rombauts, S., Rouze, P., Worden, A. Z., Robbens, S., Partensky, F., Degroove, S., Echeynie, S., Cooke, R., Saey, Y., Wuyts, J., Jabbari, K., Bowler, C., Panaud, O., Piegu, B., Ball, S. G., Ral, J.-P., Bouget, F.-Y., ... Moreau, H. (2006). Genome analysis of the smallest free-living eukaryote *Ostreococcus tauri* unveils many unique features. *Proceedings of the National Academy of Sciences of the United States of America*, 103(31), 11647–11652. <https://doi.org/10.1073/pnas.0604795103>
- Duarte, C. M., Regaudie-de-Gioux, A., Arrieta, J. M., Delgado-Huertas, A., & Agustí, S. (2013). The Oligotrophic Ocean is heterotrophic. *Annual Review of Marine Science*, 5, 551–569. <https://doi.org/10.1146/annurev-marine-121211-172337>
- Dutkiewicz, S., Scott, J. R., & Follows, M. J. (2013). Winners and losers: Ecological and biogeochemical changes in a warming ocean. *Global Biogeochemical Cycles*, 27, 463–477. <https://doi.org/10.1002/gbc.20042>
- Eppley, R. W. (1972). Temperature and phytoplankton growth in the sea. *Fishery Bulletin*, 70(4), 1063–1085.
- Evans, J. R. (1989). Photosynthesis and nitrogen relationship in leaves of C3 plants. *Oecologia*, 78, 9–19. <https://doi.org/10.1007/BF00377192>
- Falkowski, P. G., Barber, R. T., & Smetacek, V. (1998). Biogeochemical controls and feedbacks on ocean primary production. *Science*, 281, 200–207. <https://doi.org/10.1126/science.281.5374.200>
- Flombaum, P., Gallegos, J. L., Gordillo, R. A., Rincón, J., Zabala, L. L., Jiao, N., Karl, D., Li, W., Lomas, M., Veneziano, D., Vera, C., Vrugt, J. A., & Martiny, A. C. (2013). Present and future global distributions of the marine cyanobacteria *Prochlorococcus* and *Synechococcus*. *Proceedings of the National Academy of Sciences of the United States of America*, 110(24), 9824–9829. <https://doi.org/10.1073/pnas.1307701110>
- Flombaum, P., Wang, W., Primeau, F. W., & Martiny, A. C. (2020). Global picophytoplankton niche partitioning predicts overall positive response to ocean warming. *Nature Geoscience*, 13(2), 116–120. <https://doi.org/10.1038/s41561-019-0524-2>
- Fu, F.-X., Warner, M. E., Zhang, Y., Feng, Y., & Hutchins, D. A. (2007). Effects of increased temperature and CO₂ on photosynthesis, growth, and elemental ratios in marine *Synechococcus* and *Prochlorococcus* (Cyanobacteria). *Journal of Phycology*, 43(3), 485–496. <https://doi.org/10.1111/j.1529-8817.2007.00355.x>
- Grimsley, N., Pequin, B., Bachy, C., Moreau, H., & Piganeau, G. (2010). Cryptic sex in the smallest eukaryotic marine green alga research article. *Molecular Biology and Evolution*, 27(1), 47–54. <https://doi.org/10.1093/molbev/msp203>
- Henriques, M., Silva, A., & Rocha, J. (2007). Extraction and quantification of pigments from a marine microalga: A simple and reproducible method. *Communicating Current Research and Educational Topics and Trends in Applied Microbiology*, 2, 586–593.
- Heydarizadeh, P., Wafaa, B., Zahedi, M., Huang, B., Moreau, B., Lukomska, E., Couzinet-Mossion, A., Wielgosz-Collin, G., Martin-Jezequel, V., Bougaran, G., Marchand, J., & Schoefs, B. (2017). Response of CO₂-starved diatom *Phaeodactylum tricornutum* to light intensity transition. *Philosophical Transactions of the Royal Society B: Biological Sciences*, 372(1728), 20160396. <https://doi.org/10.1098/rstb.2016.0396>
- Hillebrand, H., Dürselen, C.-D., Kirschtel, D., Pollinger, U., & Zohary, T. (1999). Biovolume calculation for pelagic and benthic microalgae. *Journal of Phycology*, 35, 403–424. <https://doi.org/10.1046/j.1529-8817.1999.3520403.x>
- Irwin, A. J., & Oliver, M. J. (2009). Are ocean deserts getting larger? *Geophysical Research Letters*, 36, 1–5. <https://doi.org/10.1029/2009GL039883>
- Jin, P., & Agustí, S. (2018). Fast adaptation of tropical diatoms to increased warming with trade-offs. *Scientific Reports*, 8, 1–10. <https://doi.org/10.1038/s41598-018-36091-y>
- Kontopoulos, D. G., van Sebille, E., Lange, M., Yvon-Durocher, G., Barraclough, T. G., & Pawar, S. (2020). Phytoplankton thermal responses adapt in the absence of hard thermodynamic constraints. *Evolution*, 74(4), 775–790. <https://doi.org/10.1111/evo.13946>
- Laufkötter, C., Vogt, M., Gruber, N., Aita-Noguchi, M., Aumont, O., Bopp, L., Buitenhuis, E., Doney, S. C., Dunne, J., Hashioka, T., Hauck, J., Hirata, T., John, J., Le Quere, C., Lima, I. D., Nakano, H., Seferian, R., Totterdell, I., Vichi, M., & Volker, C. (2015). Drivers and uncertainties of future global marine primary production in marine ecosystem models. *Biogeosciences*, 12, 6955–6984. <https://doi.org/10.5194/bg-12-6955-2015>
- Leconte, J., Benites, L. F., Vannier, T., Wincker, P., Piganeau, G., & Jaillon, O. (2020). Genome resolved biogeography of Mamiellales. *Genes*, 11(1), 66. <https://doi.org/10.3390/genes11010066>
- Listmann, L., LeRoch, M., Schluter, L., Thomas, M. K., & Reusch, T. B. H. (2016). Swift thermal reaction norm evolution in a key marine phytoplankton species. *Evolutionary Applications*, 9, 1156–1164. <https://doi.org/10.1111/eva.12362>
- Litchman, E., & Klausmeier, C. A. (2008). Trait-based community ecology of phytoplankton. *Annual Review of Ecology, Evolution, and Systematics*, 39, 615–639. <https://doi.org/10.1146/annurev.ecolsys.39.110707.173549>
- Litchman, E., & Thomas, M. K. (2023). Are we underestimating the ecological and evolutionary effects of warming? Interactions with other environmental drivers may increase species vulnerability to high temperatures. *Oikos*, 2, e09155. <https://doi.org/10.1111/oik.09155>
- Liu, K., Chen, B., & Liu, H. (2022). Evidence of partial thermal compensation in natural phytoplankton assemblages. *Limnology and Oceanography Letters*, 7, 122–130. <https://doi.org/10.1002/lol2.10227>
- Lynch, M., Conery, J. S., & Galtier, N. (2003). The origins of genome complexity. *Science*, 302, 1401–1404. <https://doi.org/10.1126/science.1089370>
- Mao, Y., Guo, L., Luo, Y., Tang, Z., Li, W., & Dong, W. (2020). Sexual reproduction potential implied by functional analysis of SPO11 in *Phaeodactylum tricornutum*. *Gene*, 757, 144929. <https://doi.org/10.1016/j.gene.2020.144929>
- Marañón, E., Cermeño, P., López-Sandoval, D. C., Rodríguez-Ramos, T., Sobrino, C., Huete-Ortega, M., Blanco, J. M., & Rodríguez, J. (2013). Unimodal size scaling of phytoplankton growth and the size dependence of nutrient uptake and use. *Ecology Letters*, 16, 371–379. <https://doi.org/10.1111/ele.12052>
- Morán, X. A. G., López-Urrutia, Á., Calvo-Díaz, A., & Li, W. K. W. (2010). Increasing importance of small phytoplankton in a warmer ocean. *Global Change Biology*, 16, 1137–1144. <https://doi.org/10.1111/j.1365-2486.2009.01960.x>
- O'Donnell, D. R., Hamman, C. R., Johnson, E. C., Kremer, C. T., Klausmeier, C. A., & Litchman, E. (2018). Rapid thermal adaptation in a marine diatom reveals constraints and trade-offs. *Global Change Biology*, 24(10), 4554–4565. <https://doi.org/10.1111/gcb.14360>
- Orr, H. A. (2000). Adaptation and the cost of complexity. *Evolution*, 54(1), 13–20. <https://doi.org/10.1111/j.0014-3820.2000.tb00002.x>
- Padfield, D., & Matheson, G. (2018). Nls.Multstart: Robust non-linear regression using AIC scores. R Package. <https://CRAN.R-project.org/package=nls.multstart>, 1–5
- Padfield, D., Sullivan, H. O., & Pawar, S. (2021). rTPC and nls.Multstart: A new pipeline to fit thermal performance curves in r. *Methods in Ecology and Evolution*, 2021, 1138–1143. <https://doi.org/10.1111/2041-210X.13585>
- Padfield, D., Yvon-Durocher, G., Buckling, A., Jennings, S., & Yvon-Durocher, G. (2016). Rapid evolution of metabolic traits explains thermal adaptation in phytoplankton. *Ecology Letters*, 19, 133–142. <https://doi.org/10.1111/ele.12545>

- Palenik, B., Barahamsha, B., Larimer, F. W., Land, M., Hauser, L., Chain, P., Lamerdin, J., Regala, W., Allen, E. E., McCarren, J., Paulsen, I., Dufresne, A., Partensky, F., Webb, E. A., & Waterbury, J. (2003). The genomes of a motile marine *Synechococcus*. *Nature*, 424, 1037–1042. <https://doi.org/10.1038/nature01883.1>
- Palenik, B., Grimwood, J., Aerts, A., Rouze, P., Salamov, A., Putnam, N., Dupont, C., Jorgensen, R., Derelle, E., Rombauts, S., Zhou, K., Otiillar, R., Merchant, S. S., Podell, S., Gaasterland, T., Napoli, C., Gendler, K., Manuell, A., Tai, V., ... Grigoriev, I. V. (2007). The tiny eukaryote *Ostreococcus* provides genomic insights into the paradox of plankton speciation. *Proceedings of the National Academy of Sciences of the United States of America*, 104, 7705–7710. <https://doi.org/10.1073/pnas.0611046104>
- Pierangelini, M., Thiry, M., & Cardol, P. (2020). Different levels of energetic coupling between photosynthesis and respiration do not determine the occurrence of adaptive responses of *Symbiodiniaceae* to global warming. *New Phytologist*, 228(3), 855–868. <https://doi.org/10.1111/nph.16738>
- Pittera, J., Humily, F., Thorel, M., Garczarek, L., & Six, C. (2014). Connecting thermal physiology and latitudinal niche partitioning in marine *Synechococcus*. *The ISME Journal*, 8, 1221–1236. <https://doi.org/10.1038/ismej.2013.228>
- Ramsayer, J., Kaltz, O., & Hochberg, M. E. (2013). Evolutionary rescue in populations of *Pseudomonas fluorescens* across an antibiotic gradient. *Evolutionary Applications*, 6, 608–616. <https://doi.org/10.1111/eva.12046>
- Raven, J. A. (1994). Why are there no picoplanktonic O_2 evolvers with volumes less than $10^{-19} m^3$? *Journal of Plankton Research*, 16(5), 565–580. <https://doi.org/10.1093/plankt/16.5.565>
- Raven, J. A. (1998). The twelfth Tansley lecture. Small is beautiful: The picophytoplankton. *Functional Ecology*, 12, 503–513. <https://doi.org/10.1046/j.1365-2435.1998.00233.x>
- Reusch, T. B. H., & Boyd, P. W. (2013). Experimental evolution meets marine phytoplankton. *Evolution*, 67, 1849–1859. <https://doi.org/10.1111/evo.12035>
- Ritchie, R. J. (2006). Consistent sets of spectrophotometric chlorophyll equations for acetone, methanol and ethanol solvents. *Photosynthesis Research*, 89, 27–41. <https://doi.org/10.1007/s11120-006-9065-9>
- Samani, P., & Bell, G. (2010). Adaptation of experimental yeast populations to stressful conditions in relation to population size. *Journal of Evolutionary Biology*, 23, 791–796. <https://doi.org/10.1111/j.1420-9101.2010.01945.x>
- Schaum, C.-E., Barton, S., Bestion, E., Buckling, A., Garcia-Carreras, B., Lopez, P., Lowe, C., Pawar, S., Smirnov, N., Trimmer, M., & Yvon-Durocher, G. (2017). Adaptation of phytoplankton to a decade of experimental warming linked to increased photosynthesis. *Nature Ecology & Evolution*, 1, 0094. <https://doi.org/10.1038/s41559-017-0094>
- Schaum, C.-E., Buckling, A., Smirnov, N., Studholme, D. J., & Yvon-Durocher, G. (2018). Environmental fluctuations accelerate molecular evolution of thermal tolerance in a marine diatom. *Nature Communications*, 9, 1719. <https://doi.org/10.1038/s41467-018-03906-5>
- Schlüter, L., Lohbeck, K. T., Gutowska, M. A., Gröger, J. P., Riebesell, U., & Reusch, T. B. H. (2014). Adaptation of a globally important coccolithophore to ocean warming and acidification. *Nature Climate Change*, 4(11), 1024–1030. <https://doi.org/10.1038/nclimate2379>
- Sheehan, C. E., Baker, K. G., Nielsen, D. A., & Petrou, K. (2020). Temperatures above thermal optimum reduce cell growth and silica production while increasing cell volume and protein content in the diatom *Thalassiosira pseudonana*. *Hydrobiologia*, 847(20), 4233–4248. <https://doi.org/10.1007/s10750-020-04408-6>
- Stock, C. A., Dunne, J. P., & John, J. G. (2014). Global-scale carbon and energy flows through the marine planktonic food web: An analysis with a coupled physical-biological model. *Progress in Oceanography*, 120, 1–28. <https://doi.org/10.1016/j.pocean.2013.07.001>
- Sun, J., & Liu, D. (2003). Geometric models for calculating cell biovolume and surface area for phytoplankton. *Journal of Plankton Research*, 25, 1331–1346. <https://doi.org/10.1093/plankt/fbg096>
- Thomas, M. K., Aranguren-Gassis, M., Kremer, C. T., Gould, M. R., Anderson, K., Klausmeier, C. A., & Litchman, E. (2017). Temperature–nutrient interactions exacerbate sensitivity to warming in phytoplankton. *Global Change Biology*, 23, 3269–3280. <https://doi.org/10.1111/gcb.13641>
- Thomas, M. K., Kremer, C. T., Klausmeier, C. A., & Litchman, E. (2012). A global pattern of thermal adaptation in marine phytoplankton. *Science*, 338, 1085–1088. <https://doi.org/10.1126/science.1224836>
- Thomas, M. K., Kremer, C. T., & Litchman, E. (2016). Environment and evolutionary history determine the global biogeography of phytoplankton temperature traits. *Global Ecology and Biogeography*, 25, 75–86. <https://doi.org/10.1111/geb.12387>
- Toseland, A., Daines, S. J., Clark, J. R., Kirkham, A., Strauss, J., Uhlig, C., Lenton, T. M., Valentin, K., Pearson, G. A., Moulton, V., & Mock, T. (2013). The impact of temperature on marine phytoplankton resource allocation and metabolism. *Nature Climate Change*, 3(11), 979–984. <https://doi.org/10.1038/nclimate1989>
- Visintini, N., Martiny, A. C., & Flombaum, P. (2021). Prochlorococcus, *Synechococcus*, and picoeukaryotic phytoplankton abundances in the global ocean. *Limnology and Oceanography*, 6, 207–215. <https://doi.org/10.1002/lol2.10188>
- Willi, Y., Van Buskirk, J., & Hoffmann, A. A. (2006). Limits to the adaptive potential of small populations. *Annual Review of Ecology, Evolution, and Systematics*, 37, 433–458. <https://doi.org/10.1146/annurev.ecolsys.37.091305.110145>
- Wood, A., Everroad, R., & Wingard, L. (2005). Measuring growth rates in microalgal cultures. In R. A. Andersen (Ed.), *Algal culturing techniques*. (pp. 269–287). Elsevier.
- Zhao, P., Gu, W., Wu, S., Huang, A., He, L., Xie, X., Gao, S., Zhang, B., Niu, J., Peng Lin, A., & Wang, G. (2014). Silicon enhances the growth of *Phaeodactylum tricornutum* Bohlin under green light and low temperature. *Scientific Reports*, 4(1), 1–10. <https://doi.org/10.1038/srep03958>
- Zhong, D., Listmann, L., Santelia, M. E., & Schaum, C. E. (2020). Functional redundancy in natural pico-phytoplankton communities depends on temperature and biogeography: Phytoplankton functional redundancy. *Biology Letters*, 16(8), 20200330. <https://doi.org/10.1098/rsbl.2020.0330>

SUPPORTING INFORMATION

Additional supporting information can be found online in the Supporting Information section at the end of this article.

How to cite this article: Barton, S., Padfield, D., Masterson, A., Buckling, A., Smirnov, N., & Yvon-Durocher, G. (2023). Comparative experimental evolution reveals species-specific idiosyncrasies in marine phytoplankton adaptation to warming. *Global Change Biology*, 29, 5261–5275. <https://doi.org/10.1111/gcb.16827>